14th International Symposium on Turbulence and Shear Flow Phenomena (TSFP14)
Heidelberg, Germany, July 28–31, 2026

YO-YOING OF A VISCOELASTIC SHEAR LAYER

Giulio Foggi Rota
Giulio.FoggiRota@oist.jp

Jason Tang

Piyush Garg

Marco Edoardo Rosti

Complex Fluids and Flows Unit
Okinawa Institute of Science and Technology Graduate University
Okinawa 904-0495, Japan

ABSTRACT

We demonstrate that a mixing layer of viscoelastic fluid, such as polymer solutions, yo-yos as it develops at vanishing inertia. This stands in sharp contrast to Newtonian fluids, where the mixing layer evolves monotonically. We combine two-dimensional direct numerical simulations with a theoretical analysis of the fluid energy budget to reveal the underlying physical mechanism. The yo-yoing is shown to be driven by the (polymeric) microstructure feeding energy into the fluid whilst, in turn, being rotated by the large-scale mean shear. A mixing layer is one of the simplest and most canonical examples of unsteady flows, and we expect the mechanism described here to apply to unsteady viscoelastic flows in more complex geometries.

INTRODUCTION

Most fluids, whether encountered in biological, industrial, or geophysical settings, are not simply Newtonian but possess an internal microstructure (Bird *et al.*, 1987; Balmforth & Craster, 2001; Morozov & Spagnolie, 2015). Understanding the flows of such 'complex' fluids remains a challenging task. Viscoelastic fluids, such as polymer solutions and melts, have attracted considerable interest as a prototypical and widespread example (Bird *et al.*, 1987; Larson, 2013; Datta *et al.*, 2022; Steinberg, 2021). Viscoelastic fluids respond to external forcing with an elastic response, in addition to the usual viscous Newtonian stress, and as a result exhibit a wide variety of surprising dynamics – from novel forms of pattern formation and macro-scale behaviour (Shaqfeh, 1996; Bergeron *et al.*, 2000; Arratia *et al.*, 2006; Bhat *et al.*, 2010; Datta *et al.*, 2022) to even inertialess, elasticity-driven turbulence (Groisman & Steinberg, 2000; Larson, 2000; Steinberg, 2019, 2021; Singh *et al.*, 2024).

The microstructure of viscoelastic fluids, comprising polymer molecules, relaxes towards its equilibrium state on an intrinsic time scale (τ_p), whilst the fluid and microstructure are driven away from equilibrium by the imposed shear rate ($\dot{\gamma}$). At large Deborah numbers ($De = \dot{\gamma}\tau_p$), the microstructure strongly influences the flow, which in turn further perturbs the microstructure, giving rise to a strong coupling between the two. This two-way interaction has meant that even canonical shearing flows of viscoelastic fluids at large De, such as pressure-driven flows and mixing layers, remain poorly understood.

Viscoelastic mixing layers are characterised by momentum transfer between co-moving streams with differing velocities. Since a mixing layer describes pattern formation in a time-dependent mean–flow, understanding its roll-up has been fundamental to the dynamics of Newtonian fluids across a wide variety of settings (Ho & Huerre, 1984; Peltier & Caulfield, 2003). For viscoelastic fluids, early work on mixing layers focused on the inertial regime and concluded that viscoelasticity primarily stabilises the inertia-driven roll–up (Azaiez & Homsy, 1994*a*,*b*; Yu & Phan-Thien, 2004; Ray & Zaki, 2014). Recent experiments, conducted in two different geometries, have examined the large De mixing layer – one set for a mixing layer generated behind an obstacle inside a channel (Varshney & Steinberg, 2018; Jha & Steinberg, 2021) and the second for flow over a rigid micro-canopy (de Blois *et al.*, 2023; Lopez de la Cruz *et al.*, 2025). Both sets of experiments reported anomalous vorticity generation and turbulent-

like velocity fluctuations. However, no theoretical or numerical studies exist thus far in the parameter regime corresponding to these experiments, and an understanding of the underlying physical mechanism for these observations is still lacking. Moreover, in existing studies it is widely assumed that the time evolution of the large-scale mean–flow of the mixing layer is unaffected by viscoelasticity (Azaiez & Homsy, 1994*a*,*b*; Yu & Phan-Thien, 2004; Ray & Zaki, 2014).

In contrast, here we show that a viscoelastic mixing layer does not evolve monotonically but instead yo-yos at large De. The coupling of the microstructure to the mean–flow leads to multiple reversals of the mixing layer. We combine direct numerical simulations with a theoretical analysis of the energy budget to uncover the underlying physical dynamics, demonstrating that viscoelasticity can completely alter the time evolution of the large scales of a mixing layer.

GOVERNING EQUATIONS & SETUP

For a viscoelastic fluid, the velocity field u is governed by the Navier-Stokes equation together with the continuity equation for incompressibility. The microstructure (C) is assumed to deform affinely with the flow and is therefore modelled using the Oldroyd-B equation (Bird *et al.*, 1987; Hinch & Harlen, 2021). The governing equations are thus

$$\rho\left(\partial_t u + (u\cdot\nabla)\,u\right) = -\nabla p + \mu_f\nabla^2 u + \frac{\mu_p}{\tau_p}\nabla\cdot C,$$
$$\nabla\cdot u = 0,$$
$$\partial_t C + u\cdot\nabla C = C\cdot\nabla u + \nabla u^T\cdot C - \frac{C-\mathbf{I}}{\tau_p}.$$

where ρ is the fluid density, μ_f the fluid viscosity, μ_p the additional viscosity due to the polymers, and τ_p the relaxation time of the polymer molecules. These equations are solved in two dimensions, where x and y denote the streamwise and gradient directions respectively. Details and validation of the in-house solver employed are available on the website of the Complex Fluids and Flows Unit at OIST (`https://www.oist.jp/research/research-units/cffu/fujin`), and published by Rosti (2026). We denote the average of any variable f over the whole domain as $\langle f\rangle$, whilst $\langle f\rangle_x$ denotes the streamwise average only.

The flow is initialised with a mixing layer of thickness δ_0, confined to the centre of the domain, and a harmonic perturbation u_t of small amplitude and zero mean, such that at $t=0$, $u = U_0\tanh(2y/\delta_0)\,\hat{x} + u_t$ and $\langle u_t\rangle_x = 0$ (shown in the inset of figure 1(b)). The flow is parametrised by the Reynolds number $Re = \rho U_0\delta_0/(\mu_f+\mu_p)$), the Deborah number $De = \tau_p U_0/\delta_0$ and the viscosity ratio $\beta = \mu_f/(\mu_f+\mu_p)$, where U_0 is the initial velocity scale. For the majority of results presented, we select a parameter set of $Re = 0.2$, $De = 28$ and $\beta = 0.9$, for which inertial effects are expected to be negligible. The length scale δ_0 and time scale δ_0/U_0 are used throughout to present the results.

RESULTS

Figure 1(a) shows the variation of the absolute value of the (normalised) mean vorticity $|\langle\omega\rangle/\langle\omega_0\rangle|$ over time tU_0/δ_0, for both the Newtonian ($De=0$) and viscoelastic ($De=28$) cases, where $\langle\omega_0\rangle$ is the mean vorticity at $t=0$. Initially, the vorticity decays as the mixing layer expands due to momentum diffusion, in a manner similar to Newtonian fluids. However, a

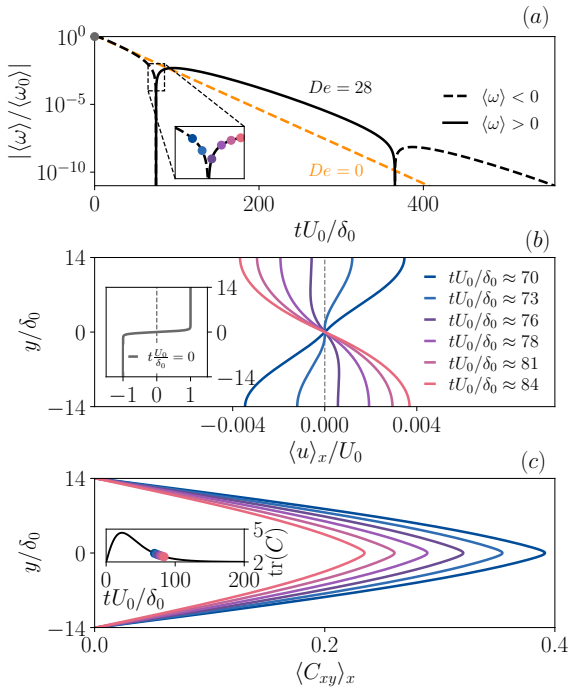

Figure 1. (a) Evolution of the absolute value of the mean vorticity $|\langle\omega\rangle/\langle\omega_0\rangle|$ with the non-dimensional time tU_0/δ_0 for the viscoelastic ($De=28$) and Newtonian cases ($De=0$). The inset is zoomed–in near the overturning time $t^*\sim 74.6$, where $\langle\omega\rangle$ changes sign. (b) The mean streamwise velocity field $\langle u\rangle_x/U_0$ versus the gradient direction y/δ_0 at various times tU_0/δ_0 near t^*; the inset shows the mixing layer at time $t=0$. (c) The spatial variation of the streamwise-averaged $\langle C_{xy}\rangle_x$ versus y/δ_0 at various times tU_0/δ_0 near t^*; the inset shows the evolution of the mean of the trace of the polymer tensor $\langle tr(C)\rangle$ over time tU_0/δ_0.

striking departure from this behaviour is observed as the mean vorticity passes through zero, changes sign, and subsequently *increases* around $tU_0/\delta_0 = t^*\sim 74.6$. The mean vorticity has thus effectively reversed sign over a very short duration around t^* – implying that the mixing layer has entirely overturned, with the streams now flowing in opposite directions to their initial configuration. Following the sign change, the mean vorticity resumes a time decay similar to that preceding the overturning. Figure 1(b) shows the gradient-direction variation of the streamwise–averaged velocity field, $\langle u\rangle_x$, at times just before and after the overturning t^*; the velocity streams indeed reverse direction. A second overturning of the mixing layer is eventually observed around $tU_0/\delta_0 = 365.4$, even as the vorticity continues to decay overall. The velocity field of a viscoelastic mixing layer thus yo-yos over time even as momentum diffuses across it. This is in sharp contrast to Newtonian mixing layers, where the mean vorticity decays monotonically over time.

Next, we examine how the flow microstructure evolves. The inset of figure 1(c) shows the time evolution of ($\langle tr(C)\rangle = \langle C_{xx}+C_{yy}\rangle$), which serves as a measure of microstructure stretching. We begin with the polymers at their equilibrium length, so $\langle tr(C)\rangle = 2$ at $t=0$. Initially, the polymers are stretched by the flow and absorb energy from it. Eventually, $\langle tr(C)\rangle$ begins to decrease, indicating that the polymers are gradually relaxing back towards their equilibrium state. Since the mean–flow is approximately unidirectional, only

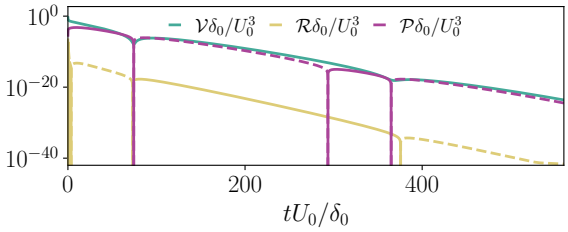

Figure 2. Evolution of the spatially averaged viscous dissipation ($\mathscr{V}\delta_0/U_0^3$), turbulent production ($\mathscr{R}\delta_0/U_0^3$) and polymer contributions ($\mathscr{P}\delta_0/U_0^3$) in the energy balance of the mean kinetic energy of the fluid over time tU_0/δ_0. Continuous lines denote positive values, dashed lines negative values.

$\langle C_{xx}\rangle_x$ and $\langle C_{xy}\rangle_x$ exhibit a non–trivial spatial variation over time, whilst $\langle C_{yy}\rangle_x \approx 1$ at all times; $\langle C_{xy}\rangle_x$ is a measure of the orientation of the microstructure. Figure 1(c) shows the gradient-direction (y/δ_0) variation of the shear component of the stress due to the microstructure, $\langle C_{xy}\rangle_x$, at various tU_0/δ_0 near the overturning time t^*. $\langle C_{xy}\rangle_x$ is largest near the centreline ($y=0$), where the mixing layer initially has the strongest velocity gradients. Nevertheless, the microstructure does not exhibit an exact mirroring of the yo-yoing of the mean velocity field at t^*.

Since there is no external energy source in the mixing layer, the yo-yoing of the mean velocity field must be driven by energy transferred from the viscoelastic microstructure. The equation governing the time evolution of the mean kinetic energy ($E = \langle\langle u\rangle_x \cdot \langle u\rangle_x\rangle/2$) may be derived from the governing equations as,

$$\frac{\mathrm{d}E}{\mathrm{d}t} = -\left\langle \left(2\frac{\mu_f}{\rho}\langle \mathbf{S}\rangle_x - \langle \mathbf{u}_t\mathbf{u}_t\rangle_x + \frac{\mu_p}{\rho\tau_p}\langle \mathbf{C}\rangle_x\right) : \langle \nabla \mathbf{u}\rangle_x \right\rangle,$$

where $u_t = u - \langle u\rangle_x$. The first and second terms on the RHS are the viscous dissipation ($\mathscr{V}$) and the turbulent production from the Reynolds stresses ($\mathscr{R}$), familiar from Newtonian fluids. The last term in the energy balance – which represents the additional energy transfer mechanism for viscoelastic fluids through coupling with the microstructure ($\mathscr{P} = \frac{\mu_p}{\rho\tau_p}\langle\langle \mathbf{C}\rangle_x : \langle\nabla\mathbf{u}\rangle_x\rangle$) – injects energy into the flow when $\mathscr{P} < 0$ and dissipates energy when $\mathscr{P} > 0$. The energy balance is exactly satisfied over the time interval considered, thereby establishing the validity of the numerical scheme.

Figure 2 shows the time evolution of the three terms. The turbulent production ($\mathscr{R}$) contributes negligibly, confirming that inertia plays no significant role. The viscous dissipation ($\mathscr{V}$) remains positive definite at all times, as expected. The yo-yoing dynamics is therefore entirely governed by the polymer coupling term $\mathscr{P}$. The time evolution of $\mathscr{P}$ allows us to infer a mechanism for the yo-yoing. Since the mean–flow is approximately unidirectional in the mixing layer, the polymer coupling term simplifies to $\mathscr{P} \approx \frac{\mu_p}{\rho\tau_p}\langle\langle C_{xy}\rangle_x\langle \mathrm{d}_y u\rangle_x\rangle$. Initially, the microstructure absorbs energy from the flow as the polymers stretch, so $\mathscr{P} > 0$ (implying both $\langle \mathrm{d}_y u\rangle > 0$ and $\langle C_{xy}\rangle > 0$). The polymers are therefore oriented along the flow direction during this phase, acting as an additional dissipative mechanism. Around $tU_0/\delta_0 = t^* \sim 74.6$, both the polymer term ($\mathscr{P}$) and the mean vorticity $\langle\omega\rangle$ change sign. For tU_0/δ_0 slightly larger than t^*, the polymer term $\mathscr{P}$ (now a production term) exceeds the viscous dissipation ($\mathscr{V}$), and the mean kinetic energy (and vorticity) can therefore grow. Thus, at t^* the polymers begin injecting energy into the fluid and drive an overturning of the mixing layer, with the two fluid streams flowing in opposite directions to before. Crucially, the reversed mean shear implies that the polymers are now oriented against the flow gradient, so $\langle \mathrm{d}_y u\rangle < 0$ whilst $\langle C_{xy}\rangle > 0$. Over time, the polymers once again become aligned with the velocity gradient of the new mixing layer and begin to dissipate energy; this occurs around $tU_0/\delta_0 \sim 293.5$ in figure 2, when $\mathscr{P}$ changes sign once more (so $\langle C_{xy}\rangle < 0$). This returns the system to a mirror image of the initial configuration, which then triggers a further overturning of the mixing layer at $tU_0/\delta_0 \sim 365.4$, and the pattern repeats.

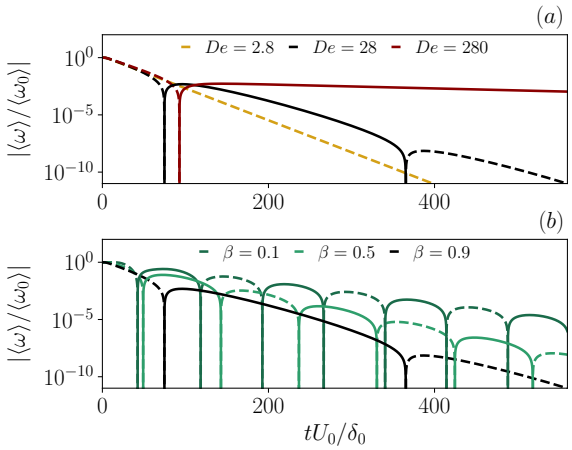

Figure 3. Evolution of the mean vorticity $|\langle\omega\rangle/\langle\omega_0\rangle|$ over time tU_0/δ_0 for varying (a) Deborah numbers (De) with $Re = 0.2$ and $\beta = 0.9$, and (b) for varying viscosity ratios (β) with $Re = 0.2$ and $De = 28$. Continuous lines denote positive values, dashed lines negative values.

The physical mechanism should be readily generalisable to any complex fluid with an orientable microstructure and a mixing layer. Indeed, the yo-yoing arises from an interplay between the decay of the mixing layer and the reorientation of the microstructure by the large-scale flow. Since the microstructure reorients between successive overturnings of the mean flow, the multiple reversals rely on the microstructure being out of synchronisation with the induced flow, with the two time scales – decay and reorientation – being comparable. If either process occurs on a markedly different time scale, multiple reversals can no longer be expected.

Nevertheless, such a two-way coupling can still be expected to persist for sufficiently elastic fluids across a wide range of parameters. Figure 3(a) and (b) show the time evolution of the mean vorticity upon varying the non-dimensional polymer relaxation time De and the polymer concentration through the viscosity ratio β, respectively. At low De (2.8), no reversal of the mixing layer occurs and the mean vorticity decays monotonically, as in the Newtonian case. Reversals are found at larger De, both for 28 and 280, establishing that $De \gg 1$ is necessary for overturning. Furthermore, at $De = 280$ the decay of the mean vorticity of the reversed mixing layer is slower and the mixing layer induced after overturning is sustained for a longer time. Upon increasing the polymer concentration, the contribution of the microstructure to the total viscosity grows, so $\beta = \mu_f/(\mu_f + \mu_p)$ decreases. The frequency of reversals increases with increasing polymer concentration, as the energy injected by the polymers can more readily overcome viscous dissipation (figure 3(b)). The overall vorticity decay is also slower at smaller β, since the reversed mixing

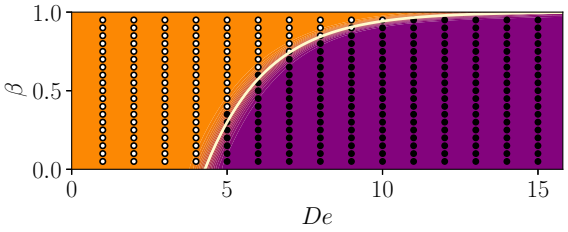

Figure 4. Parameter range over which the overturning is observed. Filled circles denote points where an overturning is found in the De-β plane, whilst open circles denote points where a monotonic decay is observed.

layer is itself induced by the microstructure.

Figure 4 shows the measured threshold De of the overturning for various β. For any β, the threshold De is seen to be higher than $O(1)$, again confirming that the overturning is an elastic effect. The time period of the oscillation is set by an interplay of two time scales - the decay of the overturned mixing layer and the time taken for the reorientation of the microstructure. Since both these processes are slower at larger De, the time period increases with De, although no simple scaling can be extracted.

CONCLUSIONS

We have demonstrated that a mixing layer in a viscoelastic fluid yo-yos at large De. Rather than the expected monotonic decay, the entire mixing layer is periodically overturned as a result of a strong two-way coupling between the microstructure and the mean–flow. Since mixing layers represent the simplest prototype for free shear flows, this striking behaviour can be expected to be quite general in unsteady viscoelastic flows. The proposed mechanism is also expected to generalise to mixing layer flows of a range of complex fluids in which the microstructure is coupled to the mean shear. Prominent examples include wormlike micelle solutions (Cates & Fielding, 2006; Fardin *et al.*, 2010), suspensions of anisotropic particles (Butler & Snook, 2018; Guazzelli & Morris, 2011), liquid crystals (Rey & Denn, 2002), and active fluids such as swimmer suspensions (Koch & Subramanian, 2011; Guasto *et al.*, 2012; Lauga, 2016). Finally, the overturning of the two streams should strongly enhance mixing relative to pure diffusion. This could be exploited in various microfluidic applications, where novel strategies are required to improve mixing in the absence of inertia (Ottino & Wiggins, 2004; Browne & Datta, 2024; Sasmal, 2025).

REFERENCES

Arratia, Paulo E, Thomas, Charles C, Diorio, James & Gollub, Jerry P 2006 Elastic instabilities of polymer solutions in cross-channel flow. *Physical Review Letters* **96** (14), 144502.

Azaiez, J & Homsy, GM 1994*a* Linear stability of free shear flow of viscoelastic liquids. *Journal of Fluid Mechanics* **268**, 37–69.

Azaiez, J & Homsy, GM 1994*b* Numerical simulation of non-newtonian free shear flows at high reynolds numbers. *Journal of non-newtonian fluid mechanics* **52** (3), 333–374.

Balmforth, NJ & Craster, RV 2001 Geophysical aspects of non-newtonian fluid mechanics. *Geomorphological Fluid Mechanics* pp. 34–51.

Bergeron, Vance, Bonn, Daniel, Martin, Jean Yves & Vovelle, Louis 2000 Controlling droplet deposition with polymer additives. *Nature* **405** (6788), 772–775.

Bhat, Pradeep P, Appathurai, Santosh, Harris, Michael T, Pasquali, Matteo, McKinley, Gareth H & Basaran, Osman A 2010 Formation of beads-on-a-string structures during break-up of viscoelastic filaments. *Nature Physics* **6** (8), 625–631.

Bird, Robert Byron, Armstrong, Robert Calvin & Hassager, Ole 1987 *Dynamics of polymeric liquids. Vol. 1: Fluid mechanics*. John Wiley and Sons Inc., New York, NY.

de Blois, Charlotte, Haward, Simon J & Shen, Amy Q 2023 Canopy elastic turbulence: Spontaneous formation of waves in beds of slender microposts. *Physical Review Fluids* **8** (2), 023301.

Browne, Christopher A & Datta, Sujit S 2024 Harnessing elastic instabilities for enhanced mixing and reaction kinetics in porous media. *Proceedings of the National Academy of Sciences* **121** (29), e2320962121.

Butler, Jason E & Snook, Braden 2018 Microstructural dynamics and rheology of suspensions of rigid fibers. *Annual Review of Fluid Mechanics* **50** (1), 299–318.

Cates, Michael E & Fielding, Suzanne M 2006 Rheology of giant micelles. *Advances in Physics* **55** (7-8), 799–879.

Lopez de la Cruz, Ricardo Arturo, Haward, Simon J & Shen, Amy Q 2025 Canopy elastic turbulence: Insights and analogies to canopy inertial turbulence. *PNAS nexus* **4** (1), pgae571.

Datta, Sujit S, Ardekani, Arezoo M, Arratia, Paulo E, Beris, Antony N, Bischofberger, Irmgard, McKinley, Gareth H, Eggers, Jens G, López-Aguilar, J Esteban, Fielding, Suzanne M, Frishman, Anna *et al.* 2022 Perspectives on viscoelastic flow instabilities and elastic turbulence. *Physical Review Fluids* **7** (8), 080701.

Fardin, Marc-Antoine, Lopez, Diego, Croso, J, Grégoire, Guillaume, Cardoso, Olivier, McKinley, Garett Huw & Lerouge, Sandra 2010 Elastic turbulence in shear banding wormlike micelles. *Physical review letters* **104** (17), 178303.

Groisman, Alexander & Steinberg, Victor 2000 Elastic turbulence in a polymer solution flow. *Nature* **405** (6782), 53–55.

Guasto, Jeffrey S, Rusconi, Roberto & Stocker, Roman 2012 Fluid mechanics of planktonic microorganisms. *Annual Review of Fluid Mechanics* **44** (1), 373–400.

Guazzelli, Elisabeth & Morris, Jeffrey F 2011 *A physical introduction to suspension dynamics*, , vol. 45. Cambridge University Press.

Hinch, John & Harlen, Oliver 2021 Oldroyd b, and not a? *Journal of Non-Newtonian Fluid Mechanics* **298**, 104668.

Ho, C-M & Huerre, Patrick 1984 Perturbed free shear layers. *Annual Review of Fluid Mechanics* **16**, 365–424.

Jha, Narsing K & Steinberg, Victor 2021 Elastically driven kelvin–helmholtz-like instability in straight channel flow. *Proceedings of the National Academy of Sciences* **118** (34), e2105211118.

Koch, Donald L & Subramanian, Ganesh 2011 Collective hydrodynamics of swimming microorganisms: living fluids. *Annual Review of Fluid Mechanics* **43** (1), 637–659.

Larson, Ronald G 2000 Turbulence without inertia. *Nature* **405** (6782), 27–28.

Larson, Ronald G 2013 *Constitutive equations for polymer melts and solutions: Butterworths series in chemical engineering*. Butterworth-Heinemann.

Lauga, Eric 2016 Bacterial hydrodynamics. *Annual Review of Fluid Mechanics* **48** (1), 105–130.

Morozov, Alexander & Spagnolie, Saverio E 2015 Introduc-

tion to complex fluids. *Complex fluids in biological systems: experiment, theory, and computation* pp. 3–52.

Ottino, Julio M & Wiggins, Stephen 2004 Introduction: mixing in microfluidics. *Philosophical Transactions of the Royal Society of London. Series A: Mathematical, Physical and Engineering Sciences* **362** (1818), 923–935.

Peltier, WR & Caulfield, CP 2003 Mixing efficiency in stratified shear flows. *Annual Review of Fluid Mechanics* **35** (1), 135–167.

Ray, Prasun K & Zaki, Tamer A 2014 Absolute instability in viscoelastic mixing layers. *Physics of Fluids* **26** (1).

Rey, Alejandro D & Denn, Morton M 2002 Dynamical phenomena in liquid-crystalline materials. *Annual Review of Fluid Mechanics* **34** (1), 233–266.

Rosti, M. E. 2026 Simulating laminar and turbulent multiphase flows with Fujin. *Fluid Dyn. Res.* **58**, 021401.

Sasmal, C 2025 Potential applications of elastic instability and elastic turbulence: A comprehensive review, limitations, and future directions. *Journal of Non-Newtonian Fluid Mechanics* p. 105393.

Shaqfeh, ES G 1996 Purely elastic instabilities in viscometric flows. *Annual Review of Fluid Mechanics* (28), 129–185.

Singh, Rahul K, Perlekar, Prasad, Mitra, Dhrubaditya & Rosti, Marco E 2024 Intermittency in the not-so-smooth elastic turbulence. *Nature Communications* **15** (1), 4070.

Steinberg, Victor 2019 Scaling relations in elastic turbulence. *Physical Review Letters* **123** (23), 234501.

Steinberg, Victor 2021 Elastic turbulence: an experimental view on inertialess random flow. *Annual Review of Fluid Mechanics* **53** (1), 27–58.

Varshney, Atul & Steinberg, Victor 2018 Mixing layer instability and vorticity amplification in a creeping viscoelastic flow. *Physical Review Fluids* **3** (10), 103303.

Yu, Zhaosheng & Phan-Thien, Nhan 2004 Three-dimensional roll-up of a viscoelastic mixing layer. *Journal of Fluid Mechanics* **500**, 29–53.